Journal of the Physical Society of Japan
Vol. 71, No. 4, April, 2002, pp. 1052–1058

Statistical Mechanics of Image Restoration by the Plane Rotator Model

Yôhei SAIKA and Hidetoshi NISHIMORI[1]

Department of Electrical Engineering, Wakayama National College of Technology, Wakayama 644-0023
[1]*Department of Physics, Tokyo Institute of Technology, Tokyo 152-8551*

(Received July 5, 2001)

On the basis of statistical mechanics formulation for problems of image restoration and error-correcting codes, we propose a new technique of image restoration for a binary image using the plane rotator model. In our formulation, the restored image is obtained from the equilibrium state of a ferromagnetic plane rotator model under a random field which consists of the corrupted image at finite temperature. The validity of our technique is evaluated by the dependence of overlap on the hyperparameters using the replica symmetric theory for the infinite-range model. The theory shows that our technique achieves the same optimal performance with that by the Ising spins. This statement is qualitatively confirmed by Monte Carlo simulations for two-dimensional images. Furthermore we estimate the dynamics of our technique by using Monte Carlo simulations. The simulations reveal that the convergence to the restored image is faster than that by the Ising model at low temperature.

KEYWORDS: statistical mechanics, image restoration, plane rotator model, replica theory, Monte Carlo simulation
DOI: 10.1143/JPSJ.71.1052

1. Introduction

For many years, a lot of researchers have been working on problems related to information processing, such as image analysis, statistics for spatial data and Markov random fields.[1–7)]

Since the paper by Geman and Geman,[8)] researchers have paid attention to the relation between the problem of image restoration and statistical mechanics. Various methods of statistical mechanics have been applied to the problem of image restoration, such as the mean-field approximation and mean-field annealing.[9–11)] Pryce and Bruce[12)] have studied the problem of image restoration on the basis of statistical mechanics at finite temperature. Also, in the problem of error-correcting codes, Rujan[13)] has proposed the technique of finite temperature decoding for Sourlas' codes,[14)] based on the statistical mechanics of spin glasses. Recently, Nishimori and Wong[15)] have constructed the statistical mechanics formulation on the basis of the equilibrium statistical mechanics of Ising spin glasses in a unified framework. Following them, Carlucci and Inoue[16)] have constructed the statistical mechanics formulation of the problem of image restoration by using the Potts spin glasses.

In the present research, on the basis of the statistical mechanics formulation, we propose a new technique for the restoration of a binary image with the use of the plane rotator model.[17)] This model is introduced in the hope that more flexible or more noise/uncertainity tolerant system may be constructed by the plane rotator which is "softer" than the Ising spin. In order to clarify the performance of the plane rotator model for the problem of image restoration, we first evaluate how the overlap between the original and restored images depends on the hyperparameters by the replica symmetric theory for the infinite-range model. This theory gives the result that the optimal performance by the plane rotator is the same as that by the Ising spin, although the Ising model has a wider region in which the optimal overlap is obtained than the plane rotator one as a function of the hyperparameters. We then confirm the above result by Monte Carlo simulations for two-dimensional images. Next, in order to understand the dynamics of image restoration (such as the basin of attraction), we study how the system converges to the restored image both by the plane rotator and Ising models. The simulations lead to the statement that the convergence to the restored image by the plane rotator model is faster than that by the Ising model in the low-temperature region.

The contents of the present paper are as follows. In §2, we develop the general formulation for the problem of image restoration using the plane rotator model. In §3, we estimate the performance of our technique for restoration by using the replica symmetric theory for the infinite-range model. In §4, in order to confirm the result of the replica symmetric theory, we carry out Monte Carlo simulations for two-dimensional images. We then evaluate the dynamics of image restoration due to the plane rotator model. §5 is devoted to summary and discussion.

2. General Formulation

In this section, on the basis of the statistical-mechanical treatment for image restoration using the Ising model,[15)] we develop our formulation of image restoration due to the plane rotator model.

Let us suppose that the original image $\{\xi_i\}$ is generated with the probability $P(\{\xi_i\})$ (the prior). Here we are considering a binary image with N pixels, $\xi_i = \pm 1$ and $i = 1, \cdots, N$. We also investigate the effects of redundant contributions (corresponding to the parity-checking term in error-correcting codes) represented by the products of neighboring pixel values $\{\xi_i\xi_j\}$, where $i, j = 1, \cdots, N$, in addition to the information of the original image. The corrupted image will be written as $\{\tau_i\}$ and the corrupted version of the redundant terms $\{\xi_i\xi_j\}$ is denoted as $\{J_{ij}\}$. We treat here two kinds of noises; binary and Gaussian noises.

2.1 *Two types of noises*

In the case of binary noise, the corrupted value τ_i (J_{ij}) is equal to $-\xi_i$ ($-\xi_i\xi_j$) with noise probability p. The conditional probability to observe the corrupted image $\{\tau_i\}$ with $\{J_{ij}\}$ given the original image $\{\xi_i\}$ is then written in a

compact form as

$$P(\{\tau_i\},\{J_{ij}\}|\{\xi_i\}) = (2\cosh\beta_1)^{-3N} \times \exp\left(\beta_1 \sum_i \tau_i\xi_i + \beta_1 \sum_{(i,j)} J_{ij}\xi_i\xi_j\right), \tag{2.1}$$

where

$$\beta_1 = \frac{1}{2}\log\frac{1-p}{p}. \tag{2.2}$$

Here (i,j) denotes the set of neighboring pixels.

We carry out the maximum posterior marginal (MPM) estimate for the restoration of the binary image. Usually, the Ising spins $\{\sigma_i\}$ ($\sigma_i = \pm 1$, $i = 1,\cdots,N$) are used in order to estimate the posterior:

$$P\big(\{\sigma_i\}|\{\tau_i\},\{J_{ij}\}\big) \propto P\big(\{\tau_i\},\{J_{ij}\}|\{\sigma_i\}\big)P\big(\{\sigma_i\}\big) \tag{2.3}$$

based on the Bayes formula. Here we set the noise probability as

$$P\big(\{\tau_i\},\{J_{ij}\}|\{\sigma_i\}\big) \propto \exp\left(h\sum_i \tau_i\sigma_i + \beta_J \sum_{(i,j)} J_{ij}\sigma_i\sigma_j\right) \tag{2.4}$$

and the model prior as

$$P\big(\{\sigma_i\}\big) = \frac{1}{Z(\beta_{\rm m})}\exp\left(\beta_{\rm m}\sum_{(i,j)}\sigma_i\sigma_j\right) \tag{2.5}$$

with $Z(\beta_{\rm m})$ the normalization factor. This model prior (or its variant) is often used in the restoration of natural images, because it suppresses different states between neighboring sites.

In the present paper, as an approximation to the posterior, we try a system of the plane rotators $\{\boldsymbol{S}_i\}$ ($S_{i1}^2 + S_{i2}^2 = 1$, $i = 1,\cdots,N$) as

$$P\big(\{\boldsymbol{S}_i\}|\{\tau_i\},\{J_{ij}\}\big) \propto \exp\left(h\sum_i \tau_i S_{i1} + \beta_J\sum_{(i,j)} J_{ij}S_{i1}S_{j1} + \beta_{\rm m}\sum_{(i,j)} S_{i1}S_{j1} + D\sum_i \big(S_{i2}\big)^2\right) \tag{2.6}$$

for more flexible and smooth restoration process than the Ising case. The original and corrupted images remain binary.

By using this posterior, the restored value of the ith pixel is obtained by estimating the sign of the mean of S_{i1} from the posterior as

$$\mathrm{sgn}\langle S_{i1}\rangle = \mathrm{sgn}\left(\frac{\sum_{\{\boldsymbol{S}_i\}} S_{i1}\exp(-H)}{\sum_{\{\boldsymbol{S}_i\}}\exp(-H)}\right), \tag{2.7}$$

where

$$H = -h\sum_i \tau_i S_{i1} - \beta_J\sum_{(i,j)} J_{ij}S_{i1}S_{j1} - \frac{1}{T_{\rm m}}\sum_{(i,j)} S_{i1}S_{j1} - D\sum_i \big(S_{i2}\big)^2. \tag{2.8}$$

The trace over $\{\boldsymbol{S}_i\}$ is actually integration over these continuous variables. Here $T_{\rm m}$ is defined by $T_{\rm m} = \beta_{\rm m}^{-1}$. We notice here that in §4 we also use the Hamiltonian:

$$H = -\frac{h}{\hat{T}_{\rm m}}\sum_i \tau_i S_{i1} - \frac{\beta_J}{\hat{T}_{\rm m}}\sum_{(i,j)} J_{ij}S_{i1}S_{j1} - \frac{1}{\hat{T}_{\rm m}}\sum_{(i,j)} S_{i1}S_{j1}. - \frac{D}{\hat{T}_{\rm m}}\sum_i \big(S_{i2}\big)^2 \tag{2.9}$$

where we rewrite h, β_J, $1/T_{\rm m}$ and D in eq. (2.8) by $h/\hat{T}_{\rm m}$, $\beta_J/\hat{T}_{\rm m}$, $1/\hat{T}_{\rm m}$ and $D/\hat{T}_{\rm m}$.

To proceed further with theoretical analysis, we have to assume some explicit form of the source prior $P(\{\xi_i\})$. Following Nishimori and Wong,[15] we adopt the Boltzmann factor of the two-dimensional Ising ferromagnet:

$$P(\{\xi_i\}) = \frac{1}{Z(\beta_{\rm s})}\exp\left(\beta_{\rm s}\sum_{(i,j)}\xi_i\xi_j\right) \tag{2.10}$$

which has a similar form to the above model prior (2.5). We will often write $T_{\rm s}$ for $\beta_{\rm s}^{-1}$.

In the case of Gaussian noise, the conditional probability to observe the corrupted image $\{\tau_i\}$ with $\{J_{ij}\}$ given the original image $\{\xi_i\}$ is written as

$$P\big(\{\tau_i\},\{J_{ij}\}|\{\xi_i\}\big) \propto \exp\left(-\frac{1}{2\tau^2}\sum_i\big(\tau_i - \tau_0\xi_i\big)^2 - \frac{1}{2J^2}\sum_{(i,j)}\big(J_{ij} - J_0\xi_i\xi_j\big)^2\right)$$
$$= \exp\left(-\frac{1}{2\tau^2}\sum_i\big(\tau_i^2+\tau_0^2\big) - \frac{1}{2J^2}\sum_{(i,j)}\big(J_{ij}^2+J_0^2\big) + \frac{\tau_0}{\tau^2}\sum_i\tau_i\xi_i + \frac{J_0}{J^2}\sum_{(i,j)}J_{ij}\xi_i\xi_j,\right). \tag{2.11}$$

2.2 *Overlap*

One of the most important quantities in the present problem is the mean overlap between restored pixels $\{\mathrm{sgn}\langle S_{i1}\rangle\}$ and the original ones $\{\xi_i\}$ averaged both over the output probability and the distribution of source image:

$$M(h,\beta_J,D,\beta_{\rm m}) = \sum_{\xi}\prod\int {\rm d}J\prod\int {\rm d}\tau P(\{\xi\})P(\{J\},\{\tau\}|\{\xi\})\xi_i\mathrm{sgn}\langle S_{i1}\rangle. \tag{2.12}$$

Note that this quantity takes unity if the restoration is completely carried out, whereas it is less than 1 if the restored result is not complete.

The overlap satisfies the following important inequality:

$$M(h,\beta_J,D,\beta_{\rm m}) \le M(\beta_1,\beta_1,-\infty,\beta_{\rm s}). \tag{2.13}$$

This inequality indicates that the optimal performance by our technique does not exceed the best value by the Ising

model ($D \to -\infty$). The proof is just a straightforward application of the method used in ref. 15 to prove a similar inequality and is not shown here explicitly.

3. Infinite-Range Model

It is instructive to investigate how the overlap M depends on hyperparameters in a solvable model. The infinite-range model may seem artificial, but it serves as a guide to the qualitative understanding of system properties.[15] The infinite-range model will be examined using the replica method.

The true prior for the infinite-range model is

$$P_{\rm s}(\{\xi_i\}) = \frac{1}{Z(\beta_s)} \exp\left(\frac{\beta_{\rm s}}{N} \sum_{i<j} \xi_i \xi_j\right). \tag{3.1}$$

Here $Z(\beta_{\rm s})$ is the partition function. Because we treat the Gaussian noise, we therefore use the corrupted information J_{ij} (τ_i) with appropriate mean J_0 (τ_0) and variance J^2 (τ^2).

The effective Hamiltonian used for restoration is

$$H = -h \sum_i \tau_i S_{i1} - \beta_J \sum_{i<j} J_{ij} S_{i1} S_{j1} - \frac{\beta_{\rm m}}{N} \sum_{i<j} S_{i1} S_{j1} - D \sum_i \left(S_{i2}\right)^2. \tag{3.2}$$

By the replica trick, the free energy is expressed as

$$-\beta\big[\langle f \rangle\big] = \lim_{N\to\infty} \lim_{n\to 0} \frac{1}{Nn} \big[\log Z\big] = \lim_{N\to\infty} \lim_{n\to 0} \frac{1}{N} \frac{\big[Z^n\big] - 1}{n}, \tag{3.3}$$

where

$$\big[Z^n\big] = \sum_{\xi} \frac{1}{Z(\beta_s)} \exp\left(\frac{\beta_s}{N} \sum_{i<j} \xi_i \xi_j\right) \times \int \prod_i \left\{ {\rm d}\tau_i \frac{1}{\sqrt{2\pi\tau^2}} \right\} \prod_{i<j} \left\{ {\rm d}J_{ij} \sqrt{\frac{N}{2\pi J^2}} \right\} \exp\left(-\frac{1}{2\tau^2} \sum_i \left(\tau_i - \tau_0 \xi_i\right)^2 - \frac{N}{2J^2} \sum_{i<j} \left(J_{ij} - \frac{J_0}{N} \xi_i \xi_j \right)^2 \right) \times \sum_{\{S_i^\alpha\}} \exp\left(-H_\alpha\right), \tag{3.4}$$

with

$$H_\alpha = -h \sum_i \sum_{\alpha=1}^n \tau_i S_{i1}^\alpha - \beta_J \sum_{i<j} J_{ij} \sum_{\alpha=1}^n S_{i1}^\alpha S_{j1}^\alpha - \frac{\beta_{\rm m}}{N} \sum_{i<j} \sum_{\alpha=1}^n S_{i1}^\alpha S_{j1}^\alpha - D \sum_i \sum_{\alpha=1}^n \left(S_{i2}^\alpha\right)^2. \tag{3.5}$$

Here S_{il}^α is the lth component of the plane rotator at the ith site of the αth replica and the square brackets $[\cdots]$ denote the configurational average. Within the replica symmetric assumption, we obtain the equations of state as

$$m_0 = \big[\xi\big] = \tanh \beta_{\rm s} m_0 \tag{3.6}$$

$$t = \big[\xi \langle S_1 \rangle\big] = \frac{1}{2\cosh \beta_{\rm s} m_0} \sum_{\xi=\pm 1} \xi \exp\left(\beta_{\rm s} m_0 \xi\right) \int {\rm D}u \frac{1}{Z_\xi} \int_0^{2\pi} {\rm d}\theta \cos\theta \exp\left(\Pi_\xi\right) \tag{3.7}$$

$$q = \big[\langle S_1 \rangle^2\big] = \frac{1}{2\cosh \beta_{\rm s} m_0} \sum_{\xi=\pm 1} \exp\left(\beta_{\rm s} m_0 \xi\right) \left(\int {\rm D}u \frac{1}{Z_\xi} \int_0^{2\pi} {\rm d}\theta \cos\theta \exp\left(\Pi_\xi\right) \right)^2 \tag{3.8}$$

$$x = \big[\langle S_1^2 \rangle\big] - \frac{1}{2} = \frac{1}{2\cosh \beta_{\rm s} m_0} \sum_{\xi=\pm 1} \exp\left(\beta_{\rm s} m_0 \xi\right) \int {\rm D}u \frac{1}{Z_\xi} \int_0^{2\pi} {\rm d}\theta \frac{1}{2} \cos 2\theta \exp\left(\Pi_\xi\right) \tag{3.9}$$

$$m = \big[\langle S_1 \rangle\big] = \frac{1}{2\cosh \beta_{\rm s} m_0} \sum_{\xi=\pm 1} \exp\left(\beta_{\rm s} m_0 \xi\right) \int {\rm D}u \frac{1}{Z_\xi} \int_0^{2\pi} {\rm d}\theta \cos\theta \exp\left(\Pi_\xi\right) \tag{3.10}$$

where

$$Z_\xi = \int_0^{2\pi} {\rm d}\theta \exp\left(\Pi_\xi\right) \tag{3.11}$$

$$\Pi_\xi = a_\xi \cos\theta + b \cos^2\theta + D \sin^2\theta \tag{3.12}$$

$$a_\xi = \xi(\tau_0 h + \beta_J J_0 t) + \beta_{\rm m} m + u\sqrt{\tau^2 h^2 + \beta_J^2 J^2 q} \tag{3.13}$$

$$b = \frac{\beta_J^2 J^2}{2} (1 + x - q). \tag{3.14}$$

We can evaluate the mean of overlap M between the original and restored images from the order parameters as

$$M = \frac{1}{2\cosh \beta_{\rm s} m_0} \sum_{\xi=\pm 1} \xi \exp\left(\beta_{\rm s} m_0 \xi\right) \int {\rm D}u \ {\rm sgn}\left(\int_0^{2\pi} {\rm d}\theta \cos\theta \exp\left(\Pi_\xi\right) \right). \tag{3.15}$$

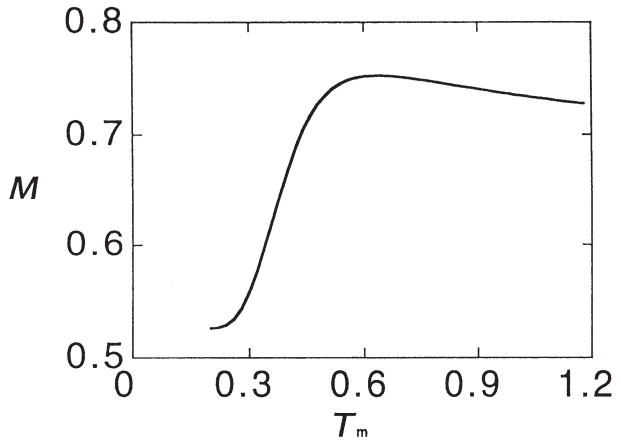

Fig. 1. The T_m-dependence of the overlap M when $T_s = 0.9$, $h = 1$, $\beta_J = 0$, $D = 0$, $\beta = 1$, $\tau_0 = \tau = 1$.

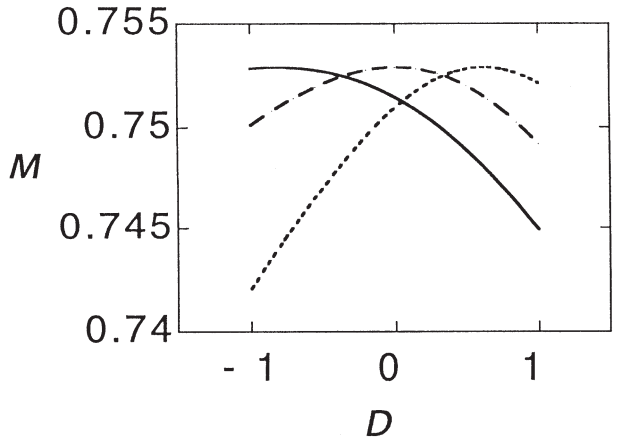

Fig. 2. Plane rotator models show the optimal overlap $M = 0.753$ for any D by tuning hyperparameter T_m. The solid/long-dashed/dotted lines corresponds to $T_m = 0.7/0.636/0.58$. Other parameters are set as $T_s = 0.9$, $h = 1$, $\beta_J = 0$, $\beta = 1$, $\tau_0 = \tau = 1$.

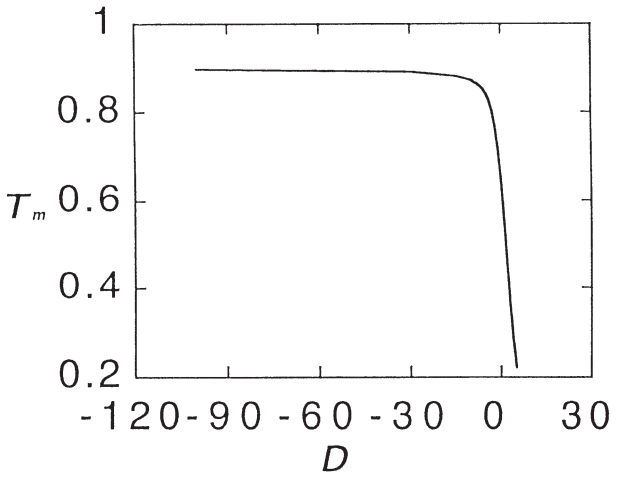

Fig. 3. The line on which the performance is optimal $M = 0.753$ on the D–T_m plane when $T_s = 0.9$, $h = 1$, $\beta_J = 0$, $\beta = 1$, $\tau_0 = \tau = 1$.

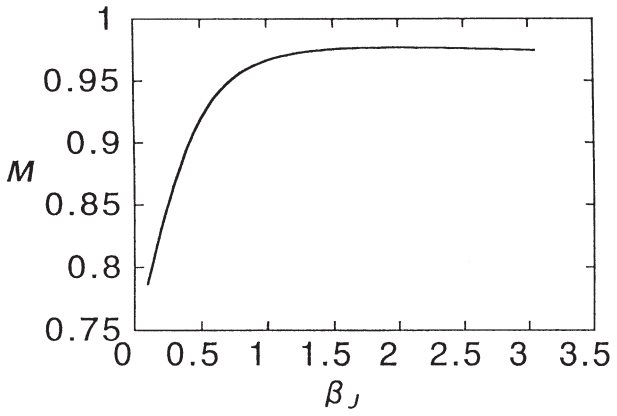

Fig. 4. The dependence of overlap M on the hyperparameter β_J when $T_s = 0.9$, $T_m = 0.636$, $h = 1$, $D = 0$, $\beta = 1$, $\tau_0 = \tau = 1$, $J_0 = J = 1$.

Figure 1 shows how the overlap M depends on T_m when $T_s = 0.9$, $h = 1$, $D = 0$, $\beta_J = 0$, $\beta = 1$ and $\tau_0 = \tau = 1$. This figure means that the present plane rotator model achieves the optimal value of the overlap $M = 0.753$ which is the same as in the Ising case.[15] However we should note that the plane rotator model shows the optimal overlap at $T_m \neq T_s$ in contrast to the Ising case.[15]

Figure 2 is the D-dependence of the overlap for fixed values of T_m. It is observed that the largest value $M = 0.753$ is achieved by any T_m. Correspondingly, as is shown in Fig. 3, we can draw a line on which the optimal overlap $M = 0.753$ is obtained on the D–T_m plane. In this figure, when D goes to $-\infty$ (the Ising limit), the plane rotator model shows the optimal overlap $M = 0.753$ at $T_m \sim T_s$. On the other hand, around $D = 0$, the optimal value is realized when $T_m < T_s$.

Next, Fig. 4 shows how the overlap M grows when we introduce the redundant term in addition to the information on original images. This figure shows that the optimal overlap grows up to $M = 0.986$ at finite β_J, where β_J is the coefficient of the redundant term as in (3.2).

4. Monte Carlo Simulation

4.1 Two-dimensional images

It is difficult to investigate the performance of our method for the problem of realistic two-dimensional image restoration by analytical methods. Therefore we have carried out Monte Carlo simulations in order to evaluate both the dependence of the overlap on the hyperparameters h, T_m, β_J and the convergence toward restored images by our method in comparison to the Ising model.

Our simulations have been carried out under the following conditions. A two-dimensional image which we treat here consists of 100×100 pixels on the square lattice. Patterns of original images are generated by the prior of the Boltzmann factor of the two-dimensional Ising ferromagnet on the square lattice at $T_s = 2.15$ which is slightly lower than the critical temperature, $T_c = 2.269$. A sample of the original images is shown in Fig. 5(a). The original images are generated by the following procedure. First, in order to obtain the equilibrium state of the two-dimensional Ising ferromagnet, we carry out the Monte Carlo simulations of 20000 Monte Carlo steps starting from the white (black) pattern. After this equilibration process, we take 50 samples of the original images with the interval of 100 Monte Carlo

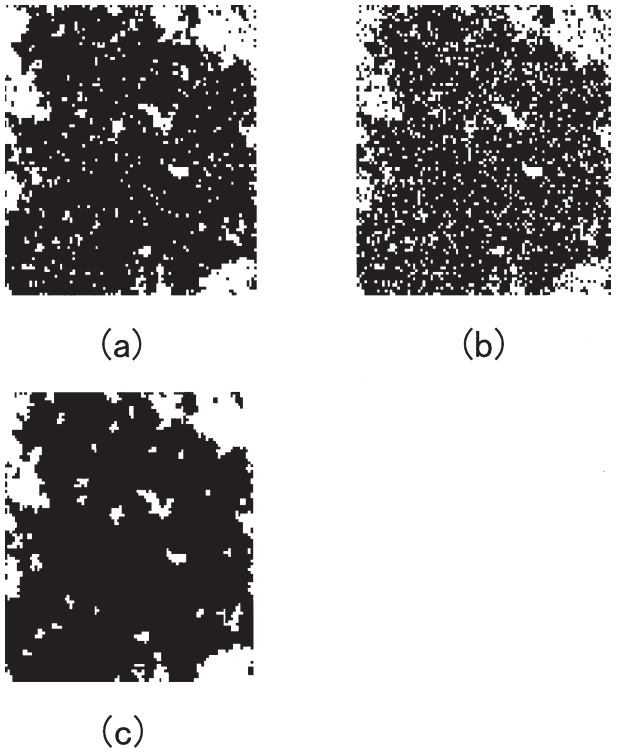

Fig. 5. A sample of two-dimensional original (corrupted, restored) image which we treat in the present research. (a) an original image constructed by the Boltzmann factor of the Ising ferromagnet on the square lattice at $T_s = 2.15$, (b) the corrupted image given the original image (a), (c) the restored image obtained from the corrupted one (b) when $h = 2.1$, $\hat{T}_m = 0.4$ and $\beta_J = 0$.

steps. Noise probability has been assumed to be $p = 0.1$. Figure 5(b) shows a sample of corrupted image obtained from the original one given in Fig. 5(a).

When we estimate the parameter dependence of the overlap by the plane rotator models, Monte Carlo simulations of 30000 Monte Carlo steps are carried out starting from the white (black) initial configuration. Figure 5(c) shows a sample restored from the corrupted image of Fig. 5(b).

When we estimate the dynamics of the plane rotator model, we observe how the overlap depends on the number of the Monte Carlo steps from the all-up configuration (or the corrupted image). Averages over 50 (20) samples are taken when we estimate the mean overlap as a function of the hyperparameters (or the number of the Monte Carlo steps) at each data point.

4.2 Parameter dependence

Here we estimate how the overlap M between the original and restored images depends on the parameters by Monte Carlo simulations from the white (black) pattern.

In the case of the Ising model, it has been shown that the optimal value of the overlap is achieved when $h = \beta_1 T_s / T_m$.[15] It has been shown in the previous section that this is not necessarily the case for the plane rotator model with infinite-range interactions. Therefore, by Monte Carlo simulations for two-dimensional images, we first estimate in Fig. 6 how the overlap M depends on h when we fix $T_m = 0.7$ and $\beta_J = 0$. Here we use the Hamiltonian (2.8) for Monte Carlo simulations of two-dimensional images in

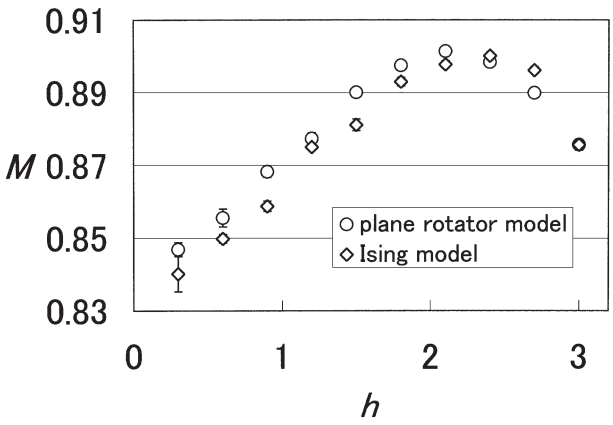

Fig. 6. The overlap M as a function of h when $T_s = 2.15$ for the temperature of the prior and $p = 0.1$ for the error probability. Here we set to $\hat{T}_m = 0.7$, $D = 0$, $\beta_J = 0$ in the case of the plane rotator model and $T_m = 2.15$, $\beta_J = 0$ in the case of the Ising model.

order to qualitatively confirm the result of the replica symmetric theory given in Fig. 1. Figure 6 shows that the plane rotator model may show the optimal overlap when $hT_m = 2.1 \neq \beta_1 T_s$, although it is not very clearly seen due to statistical uncertainty. We note that the same result as in Fig. 6 (with the initial condition of all-black image) is obtained by Monte Carlo simulations starting from restored images.

Next we examine how the overlap M depends on $\hat{T}_m$ with $h = 2.1$, $\beta_J = 0$. We use the notation of the Hamiltonian (2.9) in the following part of this section. Figure 7 shows that the overlap M monotonically increases toward its optimum value $M \sim 0.9$ with the decrease of $\hat{T}_m$ in the range $\hat{T}_m > 1.5$, and that the overlap M stays steady at its optimum value for $\hat{T}_m < 1.5$. This indicates that the MPM estimate for two-dimensional images is not always superior to the MAP estimate. Here the MAP estimate means the $\hat{T}_m \to 0$ limit of the MPM one.[15] However it also means that we do not have to lower temperature $\hat{T}_m$ than $\hat{T}_m \sim 1.5$ when we restore images by the annealing procedure. Furthermore Fig. 7 also shows that the Ising model has a wider region where the optimal overlap is obtained than the plane rotator model. A possible reason for this behavior is that the ferromagnetic region of the Ising model is wider than that of the plane

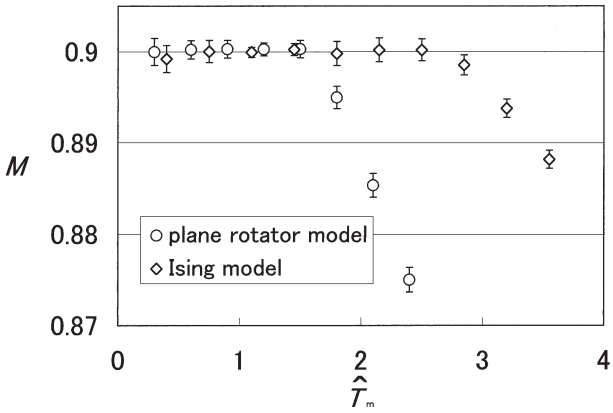

Fig. 7. The overlap M as a function of $\hat{T}_m$ when $T_s = 2.15$ and $p = 0.1$. Here we set to $h = 2.1$, $D = 0$, $\beta_J = 0$ in the case of the plane rotator model and $h = 1.099$, $\beta_J = 0$ in the case of the Ising model.

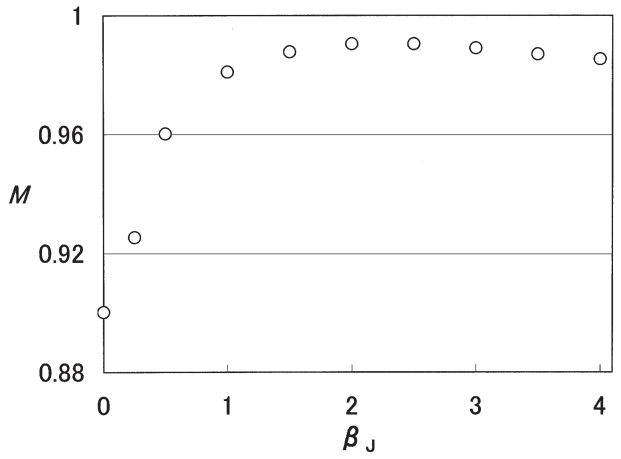

Fig. 8. The overlap M as a function of β_J by the plane rotator model when $T_s = 2.15$, $\hat{T}_m = 0.7$, $h = 2.1$, $D = 0$ and $p = 0.1$.

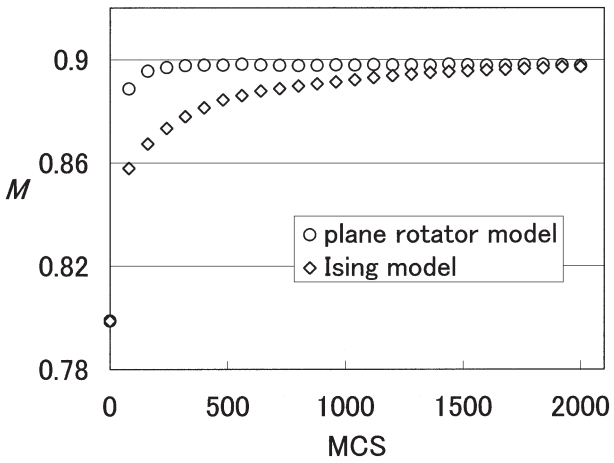

Fig. 9. The convergence from white (black) patterns to the restored images both by the plane rotator model with $h = 2.1$, $\hat{T}_m = 0.4$, $\beta_J = 0$ and by the corresponding Ising model with $h = (T_s/2)\log((1-p)/p)$, $\hat{T}_m = 0.4$, $\beta_J = 0$. Here we set to $p = 0.1$.

rotator model.

It is instructive to see how the overlap M is improved when the redundant contributions are introduced in addition to original images. Here we use the set of products of neighboring pixels as the redundunt contributions. Figure 8 shows that the plane rotator model achieves the same optimal overlap $M \sim 0.99$ with the Ising model, and that the region where the plane rotator model shows the optimal overlap spreads in $2.0 < \beta_J < 3.0$. This result means that the improvement of the optimal overlap M becomes possible by introducing redundunt contributions in addition to the information on original images also in the case of the plane rotator model. This figure also shows that the optimal β_J value cannot be obviously determined as is the case of the Ising model.

Finally, we note that the above results are obtained irrespective of the initial condition of the Monte Carlo simulations. We also notice that larger noise $p > 0.1$ case shows similar results.

4.3 *Dynamics of image restoration*

In order to estimate how images converge to restored images through the procedure due to the plane rotator model, we have used Monte Carlo simulations for two-dimensional images. We evaluate how the overlap M between the original and restored images evolves through Monte Carlo steps both with $\beta_J = 0$ and $\beta_J = 2.5$. Other parameters are set to $h = 2.1$, $\hat{T}_m = 0.4$ for the plane rotator model in this section. Figure 9 shows the convergence from white (black) patterns to the restored images both by the plane rotator model with $\beta_J = 0$ and by the corresponding Ising model. As is shown in Fig. 9, the plane rotator model needs about 160 Monte Carlo steps to reach the restored image, although the Ising model needs about 1000 Monte Carlo steps. We consider the reason for this result that the more flexible structure of the plane rotator model is effective even at low temperature. Then, we evaluate the convergence from corrupted images to the restored ones both by the plane rotator model with $\beta_J = 0$ and by the corresponding Ising model. Figure 10 shows that the plane rotator model achieves the optimal overlap faster than the Ising model in the small-$\hat{T}_m$ region, although the Ising model shows better performance until the fifth Monte Carlo step. This may be

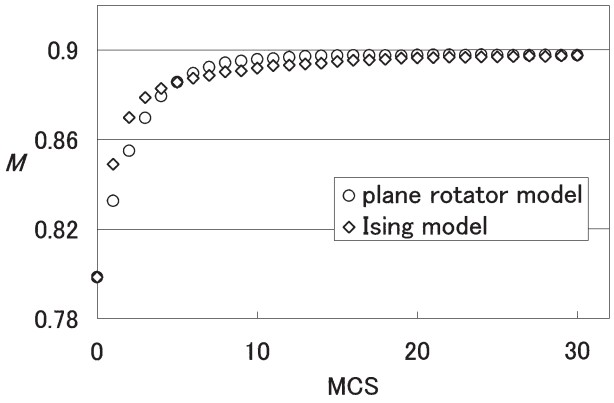

Fig. 10. The convergence from corrupted images to the restored images both by the plane rotator model with $h = 2.1$, $\hat{T}_m = 0.4$, $\beta_J = 0$ and by the corresponding Ising model with $h = (1/2)\log((1-p)/p)$, $\hat{T}_m = 0.4$, $\beta_J = 0$. Here we set to $p = 0.1$.

considered that the flexible structure of the plane rotator works more effectively in the final process of the convergence to the restored ones.

Next, we examine the effects of redundant contributions on the dynamics of the plane rotator model. Figure 11 shows the convergence from white (black) patterns to the restored images both by the plane rotator model with $\beta_J = 2.5$ and by the corresponding Ising model. This figure shows that the plane rotator model realizes the image restoration faster than the corresponding Ising model also when redundant contributions are introduced. A possible reason is that the transition from one pattern to another becomes easier due to the intermediate states between any two patterns even when the energy landscape of the system for image restoration has a glassy structure due to the redundancy. Figure 12 shows the convergence from corrupted images to the restored images both by the plane rotator model with $\beta_J = 2.5$ and by the corresponding Ising model. Similarly to the $\beta_J = 0$ case, the plane rotator model achieves the restored images faster than the Ising model, although the Ising model has better performance until the tenth Monte Carlo step.

From the above results, it is considered that the plane

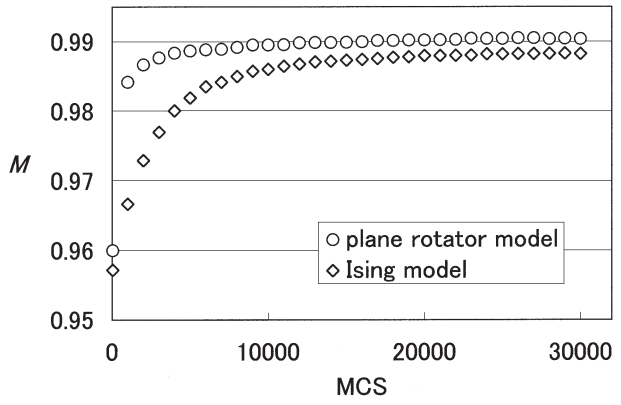

Fig. 11. The convergence from white(black) patterns to the restored images both by the plane rotator model with $h = 2.1$, $\hat{T}_{\rm m} = 1$, $\beta_J = 2.5$ and by the corresponding Ising model with $h = (T_{\rm s}/2)\log((1-p)/p)$, $\hat{T}_{\rm m} = 0.4$, $\beta_J = (T_{\rm s}/2)\log((1-p)/p)$. We set here to $p = 0.1$.

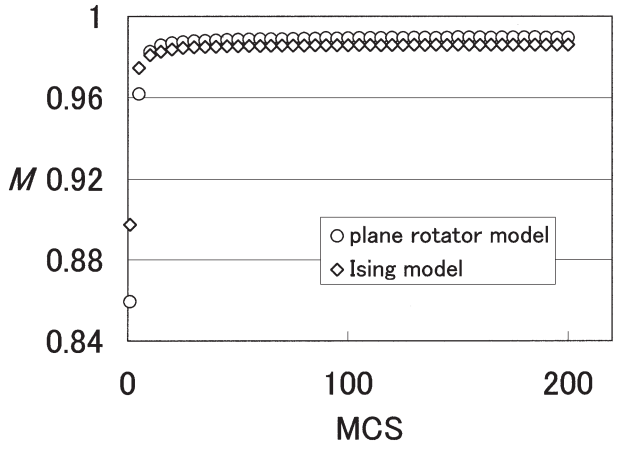

Fig. 12. The convergence from corrupted images to the restored images both by the plane rotator model with $h = 2.1$, $\hat{T}_{\rm m} = 0.4$, $\beta_J = 2.5$ and by the corresponding Ising model with $h = (T_{\rm s}/2)\log((1-p)/p)$, $\hat{T}_{\rm m} = 0.4$, $\beta_J = (T_{\rm s}/2)\log((1-p)/p)$. We set here to $p = 0.1$.

rotator model shows more smooth restoration than the Ising model in the small-$\hat{T}_{\rm m}$ region due to the flexibility of the plane rotator.

5. Summary and Discussion

In this paper, we first constructed the statistical-mechanical technique of image restoration with the use of the plane rotator model. The plane rotator model was introduced in the hope that more flexible and noise/uncertainity tolerant system may be constructed by the plane rotator which is softer than the Ising spin. Secondly, we have applied the replica-symmetric theory for the infinite-range model in order to evaluate how the overlap M between the original and restored image depends on the parameters by our technique. This theory has clarified that our technique shows the same optimal overlap $M = 0.753$ as the Ising model, although the plane rotator model shows optimal overlap when $h \neq \beta_1 T_{\rm s}/T_{\rm m}$. Thirdly, we have evaluated how the overlap M depends on the parameters $T_{\rm m}$ ($\hat{T}_{\rm m}$) and β_J by Monte Carlo simulations for two-dimensional images. From these simulations, results of the replica theory are qualitatively confirmed. It has also been shown that our technique obtains the optimal overlap $M \sim 0.90$ which is the same value as the Ising model for two-dimensional images, although the plane rotator model does not have the optimal overlap in a wider region than the Ising models in the h–$\hat{T}_{\rm m}$ space. Furthermore, we have evaluated the dynamical properties by Monte Carlo simulations. The Monte Carlo simulations have confirmed the statement that the plane rotator model shows faster convergence to the restored images than the plane rotator model when $\hat{T}_{\rm m}$ is small. The reason would be that the existence of intermediate states between arbitrary two patterns enhances transitions from one pattern to another even in the small $\hat{T}_{\rm m}$ region.

We may summarize this paper that the plane rotator model works well for image restoration in the region where the parameter $\hat{T}_{\rm m}$ is small. As a future problem, it is important to construct the algorithms to estimate the hyperparameters to give the optimal overlap with the use of plane rotator model.

1) J. Besag: J. Roy. Stat. Phys. **36** (1974) 192.
2) G. Winker: *Image analysis, Random fields and Dynamic Monte Carlo Methods, A Mathematical Introduction* (Springer-Verlag, Berlin, 1995).
3) N. A. C. Cressie: *Statistics for Spatial Data* (Wiley, New York, 1993).
4) *Spatial Statistics and Imaging*, Lecture Notes-monograph Series, Institute of Mathematical Statistics, ed. A. Possio (Hayward, Calfornia, 1991) Vol. 20.
5) R. C. Dubes and A. K. Jain: J. Appl. Stat. **16** (1989) 131.
6) Y. Ogata and M. Tanemura: Ann. Inst. Stat. Math. B **33** (1981) 315.
7) H. Nishimori: *Statistical Physics of Spin Glasses and Information Processing: An Introduction* (Oxford University Press, Oxford, 2001).
8) S. Geman and D. Geman: IEEE Trans. PAMI **6** (1984) 721.
9) D. Geiger and F. Girosi: IEEE Trans. PAMI **13** (1991) 401.
10) J. Zhang: IEEE Trans. Signal Process **40** (1992) 2570.
11) K. Tanaka and T. Morita: Phys. Lett. A **203** (1995) 122.
12) J. M. Pryce and D. Bruce: J. Phys. A **28** (1995) 511.
13) P. Rujan: Phys. Rev. Lett. **70** (1993) 2968.
14) N. Sourlas: Nature **339** (1989) 693.
15) H. Nishimori and K. Y. M. Wong: Phys. Rev. E **60** (1999) 132.
16) D. M. Carlucci and J. Inoue: Phys. Rev. E **60** (1999) 2547.
17) M. Okada, K. Doya, T. Yoshioka and M. Kawato: Tech. Rep. IEICE NC98-184 (1999) p. 239.